

Fatigue Load Reduction Potential with deformable rubber trailing edge flaps

Andreas Fischer¹, Peter Bjørn Andersen¹, Leonardo Bergami¹ and Helge Aagaard Madsen¹

asfi@dtu.dk

¹Department of Wind Energy, Technical University of Denmark, Frederiksborgvej 399, 4000 Roskilde, Denmark

Key words: Fatigue load reduction, Trailing Edge Flaps, Wind Turbine Control

1. Introduction

Most of the wind turbines being currently installed have a rated power in the MW range and rotor diameters of 100m and more. Due to the large rotor size in combination with wind shear and turbulence the rotor experiences cyclic loads which cause fatigue damage. The benefit of a reduction of the fatigue loads, especially in harsh wind conditions, is a decrease of the costs of energy, because of lower structural requirements.

Fatigue loads can be reduced by changing the local lift at the blade of the wind turbine. This can be achieved by pitching the whole blade or by equipping the blade with trailing edge flaps and changing locally the camber of the blade by flap deflection. The latter is much more energy efficient for the large blades on MW wind turbines.

In [1] a control strategy for trailing edge flaps using the local inflow vector to derive a control signal was developed. It was also demonstrated that the local inflow vector can be measured with Pitot tubes mounted on the blade in the DAN AERO experiment [2]. When the control algorithm was applied as post processing to data from simulations with the aero-elastic code HAWC2 the equivalent fatigue load of the blade normal force could be reduced significantly. If the control algorithm was applied to data obtained from measurements a significant reduction of the equivalent fatigue load of the blade normal force was achieved, but it was not as large as the one obtained for computed data. However, the potential for fatigue load reduction was huge in both cases.

In this previous investigation the aerodynamic characteristics of the flap were not part of the scope. In this paper we include the aerodynamic properties of the flap by modelling them in the computations. A BEM-based aerodynamic model to account for the steady and unsteady effects of trailing edge flap deflection was developed at DTU Wind Energy [3,4] and implemented in the aero-elastic code HAWC2 [5].

We present as well the development of a technical solution for deformable trailing edge flaps, which was initiated in 2006 at DTU Wind Energy and resulted in the design of the controllable rubber trailing edge flap (CRTEF) [6]. Due to the flexibility of the material, the flap deflection is achieved by pressurizing cavities in the flap. A prototype was developed in collaboration with the industrial partner REHAU AG (Germany) and tested in a wind tunnel in the INDUFLAP project.

2. Methods

2.1. Aero-elastic modelling

HAWC2 is an aero-elastic code for horizontal axis wind turbines [7]. The structural part is based on a multi-body formulation. Arbitrary large rotation of the bodies can be handled. The bodies are assembled of Timoshenko beam elements. The aerodynamic model is based on the classic blade element momentum theory was extended to include the effects of dynamic, skewed and sheared inflow as well as

dynamic stall effects.

The code contains a model to simulate the aerodynamic effects of trailing edge flap deflection. The model is capable of predicting the unsteady aerodynamics in attached and separated flow. The formulation for attached flow was derived by Gaunaa [3] using unsteady potential flow theory for thin aerofoils. The formulation for separated flow is based on a Beddoes-Leishman type of model for dynamic stall developed by Hansen [4]. The implementation of the model in the HAWC2 code is described by Bergami [5].

Computations were carried out for the NEG-Micon NM80 wind turbine [2]. The structural model for HAWC2 of the NM80 turbine is described in [8]. We implemented one flap on each blade. The flap is located at radial position $r=30\text{m}$ to 36m and extends over 10% of the chord lengths. The blade length measured from the centre of the hub is 40m .

NM80 turbine was run with a constant rotational speed of $\Omega=1.7\text{rad/s}$ in the simulations. The mean wind speed at hub height was 10m/s and wind shear was described by a power law with an exponent of 0.1. The spectral characteristics of inflow turbulence are described by the Mann turbulence model [9] in HAWC2. The length scale L of the Mann turbulence model was set to $L=29.4\text{m}$ and the eddy life time parameter to $\Gamma=3.9$ according to the recommendation for neutral atmospheric conditions in [7]. Several simulations with different turbulence intensity were run, but we used the same turbulence seed in all simulations.

2.2. Aerodynamic modelling of Trailing Edge Flaps

The model for the unsteady aerodynamic behaviour of the blade with flap needs as input the steady lift drag and moment coefficients as function of the angle of attack α and the flap set angle β . CFD computations [10] were performed for the NACA64_A17 aerofoil with a flap extending over 10% of the chord length. The aerodynamic properties of the NACA64_A17 aerofoil are very close to those of the aerofoils used on the outer part of the wing of the NM80 turbine and the flap is assumed to have a similar deflection shape. Due to the high computational costs of CFD it was not possible to make computation for the NM80 aerofoil section with flap. Instead, we assumed that the change in lift coefficient as function of the flap set angle is the same as for the NACA64_A17 aerofoil. With this assumption we computed the aerofoil polar as function of angle of attack and flap set angle.

2.3. Flap Control Strategy

The ideal feed forward control algorithm uses the measured relative velocity V_r and angle of attack α at a blade section to control the normal force F_N . The relation between the normal force F_N and the inflow V_r and α is given by

$$F_N = \frac{1}{2} \rho V_r^2 C_N(\alpha) c$$

where C_N is the normal force coefficient and c is the chord length of the blade section. Hence, controlled force becomes

$$F_{Nc} = F_N - f_c V_r^2$$

The control parameter f_c can then be derived by a Reynolds decomposition of the variables F_N , V_r and C_N in equation 1 into mean and fluctuating part. It reads

$$f_c = K_\alpha (\alpha - \bar{\alpha}) + K_{V_r} \frac{V_r^2 - \bar{V}_r^2}{V_r^2}$$

K_α and K_{V_r} are control constants determined by numerical optimization. The numerical optimization minimizes the objective function $(\overline{F_{Nc}^2})$. The overline denotes the mean value which is derived in practice by band stop filtering the time signal of the quantity. We applied an ideal band stop filter with a frequency window of 0.1-0.95Hz. This band width contains the frequency content of 1, 2 and 3 times the rotational frequency.

The flap set angle is derived with equation in the following way: The controlled lift force coefficient C_{Lc} is

computed from the controlled normal force coefficient C_{Nc} . The aerodynamic data is tabulated as function of the angle of attack α and the flap set angle β . With known angle of attack α and the target lift coefficient C_{Lc} the flap set angle can be interpolated. Once the flap angle is computed, the simulation is re-run and the flap set angle is fed to the controller as prescribed time series.

2.4. Flexible Trailing Edge Flaps

A continuous deformation of the trailing edge is aerodynamically better behaved than a discontinuous deformation resulting of the deflection of a rigid flap [11]. Hence, the design of trailing edge flaps built of flexible material was initiated at DTU Wind Energy in 2006. This effort led to trailing edge flaps built from rubber material [6], Figure 1.

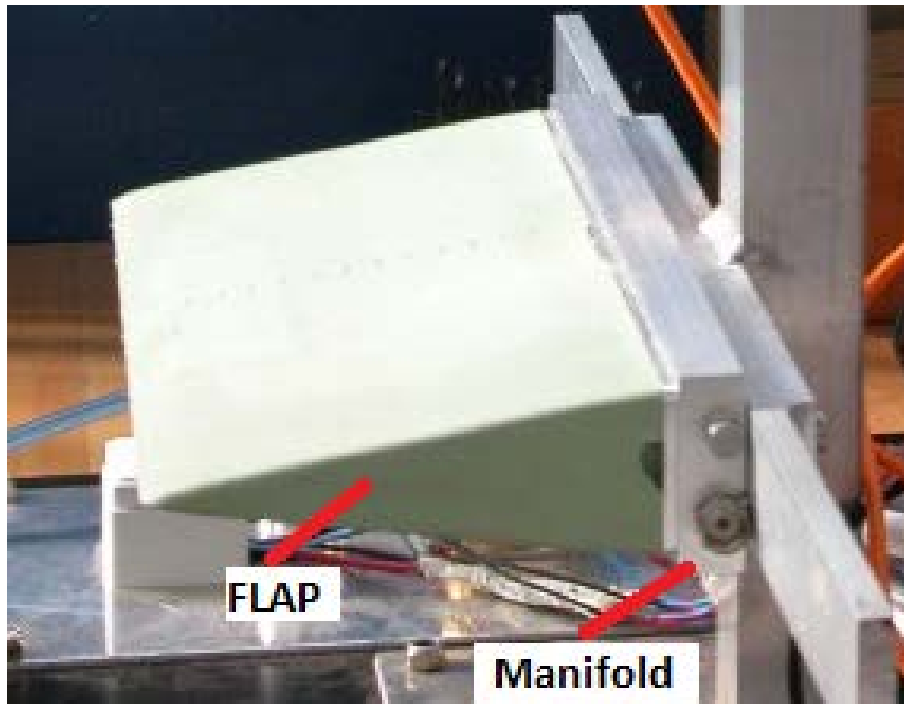


Figure 1: The rubber trailing edge flap

The flap prototype is 150mm long and based on the geometry of the NACA0015 aerofoil. The deformation of this flap is achieved by pressurizing the cavities shown in Figure 1. The cavities have a rounded shape for optimal stress distribution.

3. Results

3.1. Flap properties

Comsol [12] was used for finite element modelling of the deflection of the flap. The flap was discretized with a grid consisting 25000 tetrahedral elements. Figure 2 shows the deflection of the rubber trailing edge flap if an overpressure of 6 bar is applied in the upper cavities.

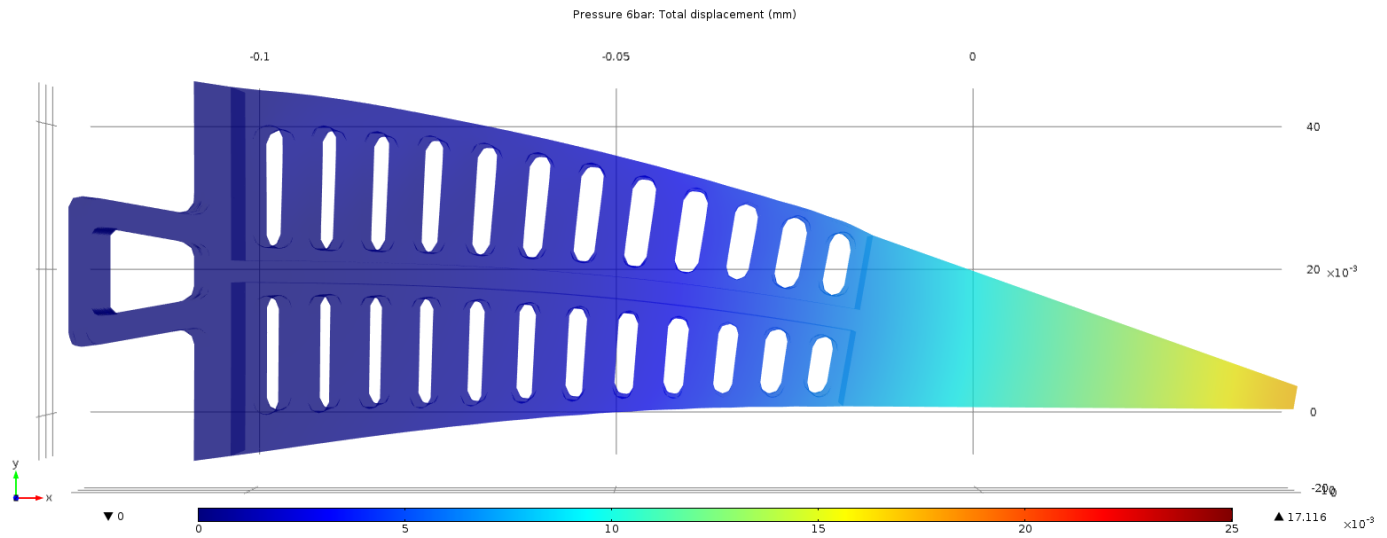


Figure 2: Deformation of the rubber trailing edge flap with 6 bar overpressure in upper cavities

The computation predicted a deflection of the flap of 8.2° . Hence, we restricted the flap set angle in the HAWC2 simulations to $\pm 8^\circ$.

3.2. Blade section aerodynamic forces

The lift coefficient of the blade section at radial position $r=33\text{m}$ computed in the simulation with 10% turbulence intensity is shown in Figure 3. The trailing edge flap changes the aerodynamic properties of the blade section in a way to obtain a more even lift distribution. Variations are significantly reduced.

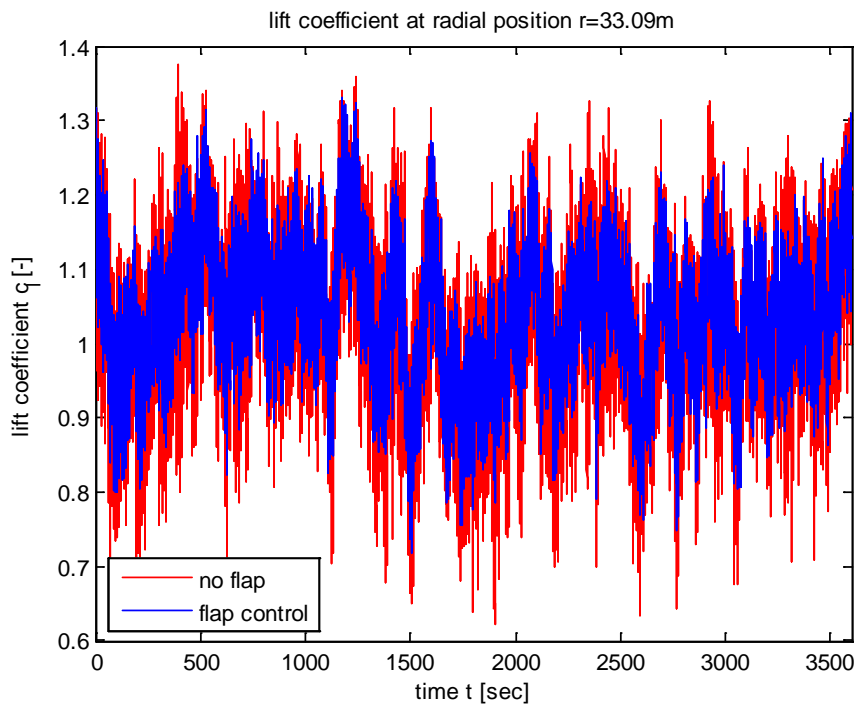
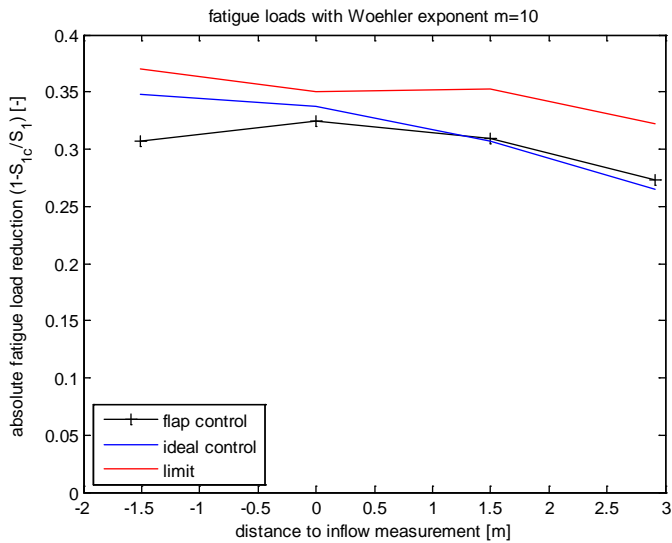
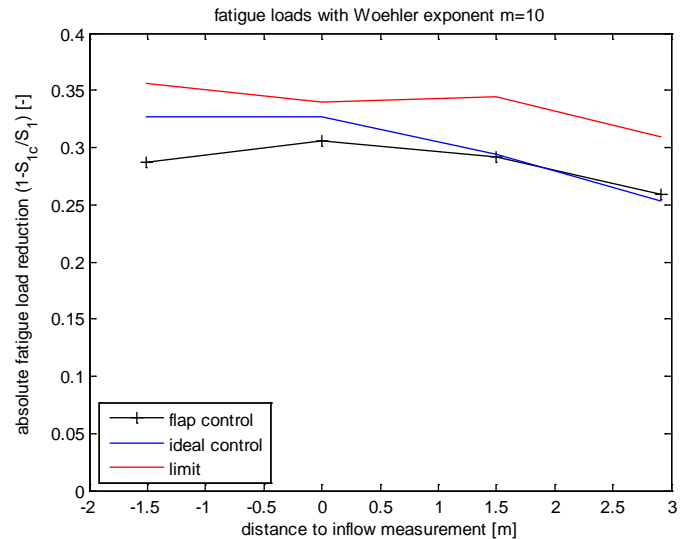


Figure 3: Lift coefficient of the blade section at $r=33\text{m}$ from simulation with turbulence intensity $Ti=0.1$

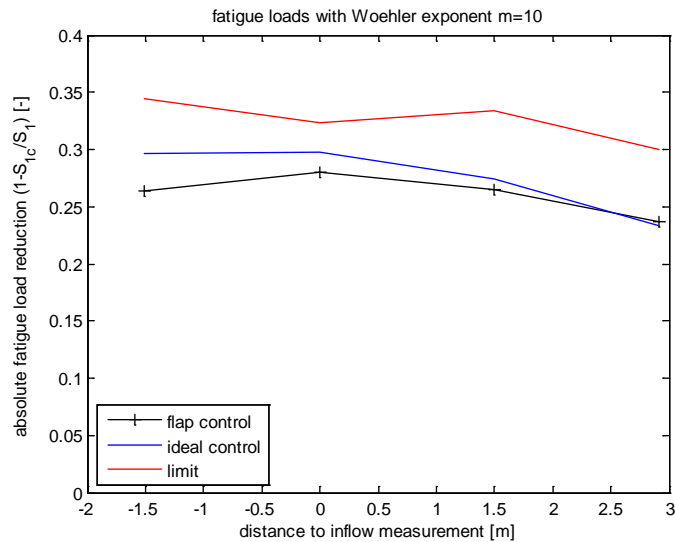
The reduction of the variations in lift coefficient results directly in a reduction of the blade normal force fluctuation. The equivalent fatigue load of the blade normal force was computed with a rainflow counting algorithm. As equivalent fatigue load (EFL) we define a sinusoidal load with the period of 1Hz and amplitude which causes the same fatigue damage to the blade as the computed normal force time series according to the theory of Palmgren-Miner and Wöhler. The fatigue load reduction is then found by comparing the EFL of the result of the simulation without flap and the result of the simulation with flap. The reduction of the EFL for different levels of turbulence intensity is depicted in Figure 4.



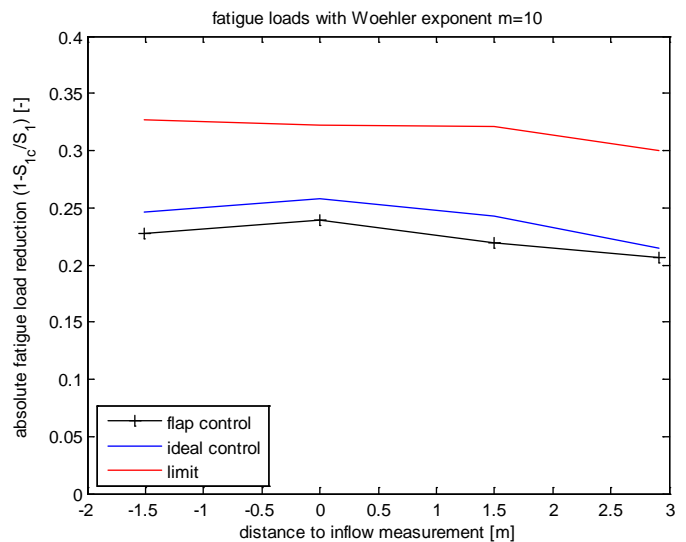
b) Ti=0.1



a) Ti=0.12



c) Ti=0.15



d) Ti=0.2

Figure 4: Fatigue load reduction of the blade normal force with respect to the distance from the inflow measurement position (inflow measured at $r=33m$)

The red line marks the maximum achievable EFL reduction in the control band width of 0.1Hz to 0.95Hz. It was computed by filtering the blade normal force time series with an ideal notch filter with the control band width as corner frequencies and the applying the rainflow counting algorithm on the filtered data. The blue line is the limit given by ideal control as described in [1]. It represents a flap with unrestricted aerodynamic capabilities and a flap actuator without time delay and unlimited actuation speed. The difference between the ideal control and the flap control is caused by the unsteady aerodynamic behaviour of the flap and the limitation in flap set angle.

With increasing turbulence intensity the maximum achievable EFL reduction decreases. The fluctuations with frequencies outside the control band width gain a stronger weight in the rainflow counting. The difference between absolute limit and ideal control becomes larger with increasing turbulence intensity. The difference between ideal control and flap control is small. Only for the highest turbulence intensity level ($Ti=0.2$) we can observe a significant difference.

3.3. Flap set angle

The prescribed flap set angle for the simulations with different turbulence intensity is displayed in Figure 5.

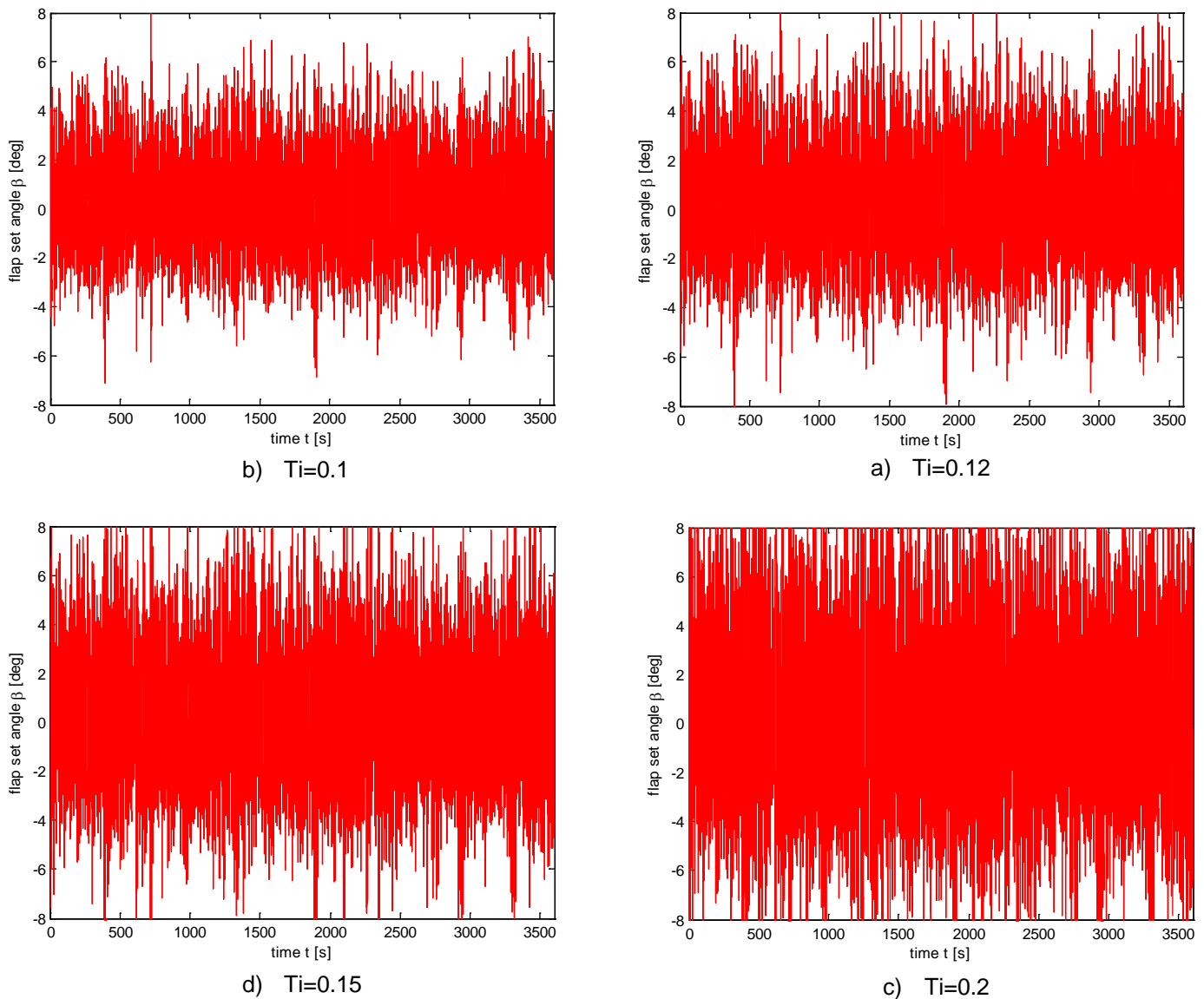


Figure 5: Prescribed flap set angle

The limit of $\pm 8^\circ$ is only restrictive in simulations with high turbulence intensity levels. For $Ti=0.2$ saturation is reached for considerable fraction of the total time. However, the effects on the EFL reduction potential, Figure 4, are small. A turbulence intensity level of $Ti=0.2$ with a wind speed of 10m/s is rather high. Hence, the flap deflection of $\pm 8^\circ$ achieved by the current flap design of DTU wind energy seems to be sufficient for most operational conditions such a wind turbine will face.

3.4. Blade root bending moment

The blade root bending moment is given by the integration of the blade sectional normal force along the blade. In this integration process the high frequency content of the normal force is filtered out, because its correlation length is small compared to the blade length. The low frequency contents will be reflected in the blade root bending moment and the reduction of the EFL of the normal force by the flap should be followed by a reduction of the EFL of the blade root bending moment.

The time series of the blade root bending moment with and without flap control for the simulation with turbulence intensity $Ti=0.1$ is shown in Figure 6.

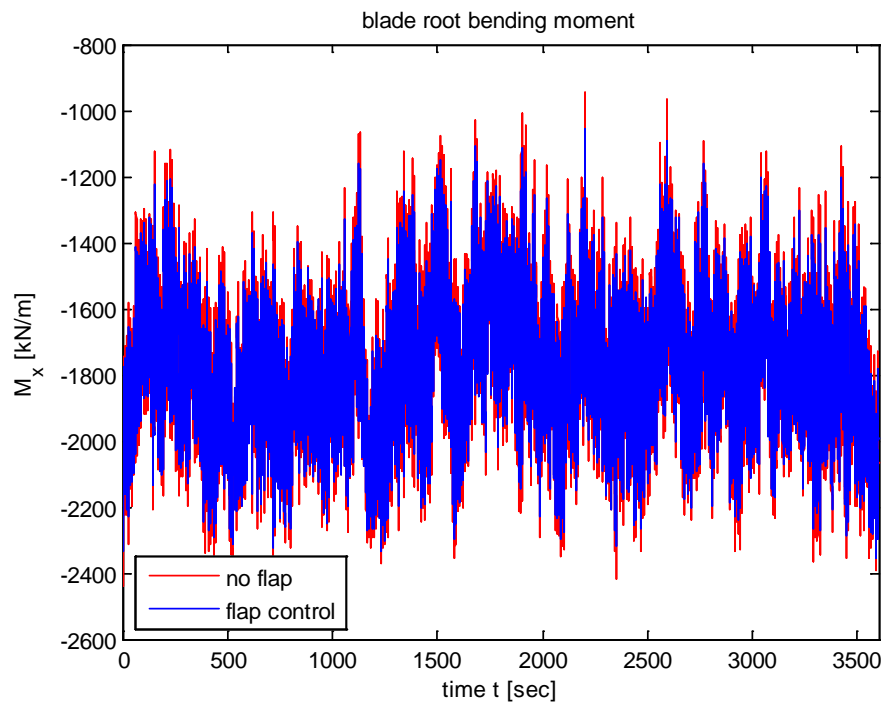


Figure 6: The blade root bending moment from simulation with turbulence intensity $Ti=0.1$

The fluctuations are not as significantly reduced as it was the case for the normal force. The spanwise extend was only 15% of the blade length. A larger flap section or more flap sections on the blade will give a higher reduction of the fluctuations of the blade root bending moment. This will be subject of future investigations.

The reduction of the EFL of the blade root bending moment is listed in Table 1 as function of the turbulence intensity level. A reduction of the EFL of more than 10% is achieved with a comparably small flap section. That is about 25% of the maximum achievable EFL reduction which can be achieved within the control band width. It illustrates the huge potential of this method for fatigue load reduction.

The EFL reduction with flap varies less than the maximum obtainable EFL reduction with changing turbulence intensity level. Even for $Ti=0.2$, when the maximum flap deflection angle constraints the flap

control, we observe no significant drop in the reduction of the EFL. It continues to follow the linear trend observed for lower turbulence intensity levels.

Ti [%]	10	12	15	20
EFL red. Flap [%]	13.42	13.15	12.24	10.88
EFL red. limit [%]	42.31	40.96	39.63	38.83

Table 1: Reduction of EFL of the blade root bending moment

4. Conclusions

Aero-elastic simulations were performed to investigate the potential to reduce fatigue loads of the blade normal force and the blade root bending moment with trailing edge flaps. The flap was controlled with the measured relative velocity and angle of attack at the blade. The flap extends from radial spanwise position 30m to 36m of a 40m long blade and the chord length was 10% of the blade chord length at the respective radial position. A prototype of a rubber trailing edge flap has been developed at DTU Wind Energy since 2006. Finite element computations showed that deflections of up to 8.2° could be achieved. Hence, the flap deflection limit in the simulation was set to $\pm 8^\circ$.

In the best case the EFL of the blade normal force could be reduced by 32.4% which corresponds to 92.7% of the achievable EFL reduction. The fatigue load reduction potential decreased with increasing turbulence intensity. For the highest simulated turbulence intensity level 20%, the EFL could be reduced by 24.0% corresponding to 74.5%. This was partly due to the fact the flap deflection limit constrained the control, but also due to the fact that the weight of the fluctuations within the control band width in the rainflow counting decreased.

The EFL of the blade root bending moment could be decreased by 13.4% in case of the lowest turbulence intensity level (10%). The value dropped to 10.9% for the highest turbulence intensity level (20%). Considering that the flap covers only 15% of the length of the blade, this is a very good achievement.

The studies showed that the fatigue load reduction potential with trailing edge flaps is not limited by the aerodynamic characteristics of the flap and deflection constraints. In a setup considering these two characteristics reductions close to the ideal limit were obtained. The next step is now to investigate how the phase lag introduced by a real time filter (necessary in a real controller setup) and the flap movement constraints imposed by the flap actuator will decrease the fatigue load reduction potential.

Acknowledgements

References

- [1] Fischer A, Madsen HAa, "Investigation of the maximum load alleviation potential using trailing edge flaps controlled by inflow data", The science of making torque from wind, Oldenburg, Germany, 2012.
- [2] Madsen HAa, Bak C, Paulsen U, Gaunaa M, Fuglsang P, Romblad J, Olesen N, Enevoldsen P, Laursen J, Jensen L, "The DAN-AERO MW Experiments: Final report". Tech. Rep. Risø-R-1726(EN), Risø National Laboratory – Technical University of Denmark, 2010.
- [3] Gaunaa M, " Unsteady two-dimensional potential-flow model for thin variable geometry airfoils", *Wind Energy*. 2010; **13**:167–192.
- [4] Hansen MH, Gaunaa M, Madsen HAa. A Beddoes–Leishman type dynamic stall model in state-space and indicial formulations. Technical Report Risø-R1354(EN), June 2004.

- [5] Bergami L, Gaunaa M. *ATEFlap* Aerodynamic Model, a dynamic stall model including the effects of trailing edge flap deflection. Technical Report Risø-R1792(EN), Feb 2012.
- [6] Madsen HA, Beller C, Andersen TL, "Development of Trailing Edge Flap Technology at DTU Wind." Sandia National Laboratories 2012, Wind Turbine Blade Workshop, United States, 29-05-12.
- [7] Larsen TJ and Hansen A, "How to HAWC2, the users manual", Tech. Rep. Risø-R-1597(ver.4-3)(EN), DTU Wind Energy – Technical University of Denmark, 2012.
- [8] Hansen M H, Fuglsang P and Thomsen K , "Aeroelastic modeling of the NM80 turbine with HAWC." Tech. Rep. Risø-I-2017(EN)(Confidential) DTU Wind Energy– Technical University of Denmark, Roskilde, Denmark, 2004.
- [9] Mann J. "The spatial structure of neutral atmospheric surface-layer turbulence." J. of Fluid Mech. 1994; **273**:141–168.
- [10] Gaunaa M, Riziotis V, Timmer N, Snel H, Andersen PB, Heinz J, "Comparison of code performance for computation of unsteady 2D aerodynamics of airfoils with deformable trailing edges." Tech. Rep. Project Upwind, 2011.
- [11] Troldborg N, "Computational study of the RisøB1-18 airfoil with a hinged flap providing variable trailing edge geometry", Wind Engineering, 2005; **29**:89–113.
- [12] COMSOL Multiphysics: www.comsol.com/products/multiphysics/